

Porous Tin Oxide Nanostructured Microspheres for Sensor Applications

Carlos J. Martinez,^{*,†} Bernard Hockey,[‡] Christopher B. Montgomery,[†] and Steve Semancik[†]

Chemical Science and Technology Laboratory and Materials Science and Engineering Laboratory, National Institute of Standards and Technology, Gaithersburg, Maryland 20899-8362

Received January 14, 2005. In Final Form: May 26, 2005

We have sought to enhance the sensitivity of conductometric gas microsensors through the design and fabrication of porous, three-dimensional tin oxide nanoparticle structures. Electrostatically controlled layer-by-layer processing in aqueous solutions was used to decorate sacrificial latex microspheres with Sb:SnO₂ nanoparticles. To evaluate their sensing performance, these structures were then deposited as films, via micropipetting, on MEMS micro-hot-plate platforms with interdigitated electrodes. Prior to gas testing, rapid heating of the micro-hot-plates was used to remove the sacrificial latex templates, thereby revealing a 3-D structure composed of interconnected spherical tin oxide nanoparticle shells with porous ultrathin walls. Changes in film conductance, caused by exposure to test gases (methanol, carbon monoxide, benzene, water) in a dry air background, were measured at different temperatures. Hollow nanoparticle microsphere films exhibited partial selectivity for these different gases, good dynamic range at different temperatures and gas concentrations, and good repeatability and stability over long runs. These films also yielded approximately 3-fold and 5-fold increases in sensitivity to methanol when compared to SnO₂ polycrystalline chemical vapor deposition films and Sb:SnO₂ microporous nanoparticle films, respectively. Gains in sensitivity are attributed to the multiscale porous architecture of the hollow microsphere films. This architecture promotes gas diffusion and increases the active surface area.

1. Introduction

There is great interest in maximizing the sensitivity of chemical sensing devices for applications such as homeland security and process control in industrial manufacturing. Films prepared from metal oxides (e.g., tin oxide (SnO₂)¹ and titanium oxide (TiO₂)²) are often the materials of choice for conductometric gas sensing because they are thermally and environmentally stable and demonstrate good reversibility in their response.³ Sensing is performed with these materials by measuring changes in electrical conductance produced by adsorption on and reaction at the surface of the metal oxide at elevated temperatures. Because sensing with these materials relies on interactions with the surface, one strategy to enhance their sensitivity is to maximize the surface area to increase the number of active surface sites.¹

Nanoscale metal oxides, especially nanoparticles, have gained much attention as potential building blocks of sensing films due to their inherently high specific surface area. Compared to those achieved using thick compact films prepared by screen printing and chemical vapor deposition (CVD) methods,⁴ superior sensitivities have been achieved using microporous and mesoporous SnO₂ and TiO₂ nanoparticle films fabricated by screen printing,⁵ spin coating,⁶ dip coating,⁷ and drop deposition.⁸ Films prepared using these methods, however, usually do not

have a well-defined porous structure, as they are usually composed of interconnected aggregates of different length scales. Because of this, a part of the surface area is lost to interparticle contacts, and furthermore, analyte diffusion to the remaining active surface area is restricted by the small pores and tortuous pathways, leading to less than optimal sensitivities. By assembling nanoparticles into an open, well-defined structure with multimodal porosity on the macro-, meso-, and microscales, it may be possible to increase the active surface area and the analyte diffusion, improving sensitivity.

A feasible way to assemble nanoparticles into complex structures is through colloidal templating.⁹ This method utilizes colloidal units as templates on which one deposits other materials to form well-controlled structures. Examples include the fabrication of inverse opals via the infiltration of a colloidal crystal¹⁰ or the layer-by-layer (LbL)¹¹ deposition of nanoparticles (e.g., SiO₂, TiO₂, SnO₂) onto sacrificial microspheres to form hollow microspheres.^{12,13} Carusso et al. fabricated porous SiO₂ hollow microspheres via the LbL deposition of polyelectrolytes and SiO₂ nanoparticles on the surface of latex microspheres, which served as sacrificial templates.¹² Xia et al. fabricated hollow SnO₂ and TiO₂ microspheres by infil-

* Corresponding author.

† Chemical Science and Technology Laboratory.

‡ Materials Science and Engineering Laboratory.

(1) Barsan, N.; Weimar, U. *J. Phys.: Condens. Matter* **2003**, *15*, 813.
 (2) Traversa, E.; Vona, M. L. D.; Licoccia, S.; Sacerdoti, M.; Carotta, M. C.; Crema, L.; Martinelli, G. *J. Sol-Gel Sci. Technol.* **2001**, *22*, 167.
 (3) Park, C. O.; Akbar, S. A. *J. Mater. Sci.* **2003**, *38*, 4611.
 (4) Cavicchi, R. E.; Semancik, S.; DiMeo, F., Jr.; Taylor, C. J. *J. Electroceram.* **2003**, *9*, 155.
 (5) Xu, C.; Tamaki, J.; Miura, N.; Yamazoe, N. *Sens. Actuators, B* **1991**, *3*, 147.

(6) Cavicchi, R. E.; Walton, R. M.; Aquino-Class, M.; Allen, J. D.; Panchapakesa, B. *Sens. Actuators, B* **2001**, *77*, 145.

(7) Kim, J. H.; Kim, S. H.; Shiratori, S. *Sens. Actuators, B* **2004**, *102*, 241.

(8) Fau, P.; Sauvan, M.; Trautweiler, S.; Nayral, C.; Erades, L.; Maisonnat, A.; Chaudret, B. *Sens. Actuators, B* **2001**, *78*, 83.

(9) Velev, O. D.; Jede, T. A.; Lobo, R. F.; Lenhoff, A. M. *Nature* **1997**, *389*, 447.

(10) Braun, P. V.; Wiltzius, P. *Nature* **1999**, *402*, 603.

(11) Sukhorukov, G. B.; Möhwald, H.; Decher, G.; Lvov, Y. M. *Thin Solid Films* **1996**, *284*, 220.

(12) Caruso, F.; Caruso, R. A.; Möhwald, H. *Science* **1998**, *282*, 1111.

(13) Zhong, Z.; Yin, Y.; Gates, B.; Xia, Y. *Adv. Mater.* **2000**, *12*, 206.

(14) Hyodo, T.; Sasahara, K.; Shimizu, Y.; Egashira, M. *Sens. Actuators, B* **2005**, *106*, 580.

trating a polystyrene colloidal crystal with a sol, removing the polystyrene microspheres using solvents, and then redispersing the microspheres in DI-H₂O.¹³

One of the first reports of using these techniques to fabricate sensor films with a well-defined porous structure was from Egashira et al.^{14,15} Macroporous sensor films were fabricated by infiltrating a 3-D array of PMMA microspheres, prepared by dip coating, with SnO₂ and TiO₂ precursors, followed by the removal of the PMMA microspheres by heating at 400 °C and calcination at 600 °C. The resulting macroporous structure provides an enhancement in both active surface area and analyte diffusion throughout the film. These films exhibited good sensitivity to H₂ and NO_x. While this work illustrates the performance benefits of macroporous sensing films, considerable work will be required to improve the fabrication methods and tailor final microstructures. A possible alternate way to achieve these goals is to use the LbL deposition technique to make SnO₂ nanoparticle-decorated latex microsphere suspensions from which sensor films can be deposited via drop deposition or spin coating. After removal of the microsphere templates, the films can be expected to consist of interconnected hollow metal oxide nanoparticle microspheres. Such films will possess a multiscale porous architecture comprised of macropores ($r_{\text{pore}} > 50$ nm) within and between the microspheres, and microporosity ($r_{\text{pore}} < 5$ nm) and mesoporosity ($r_{\text{pore}} = 5-50$ nm) in the nanoparticle shell. These structures would enhance both the available active surface area and the efficiency of analyte diffusion. Because the microspheres are processed in solution, there are several advantages to using the LbL technique. For example, it is easier to selectively deposit films on small sensing areas, such as those encountered when using micro-hot-plate microsensor (100 μm × 100 μm) platforms.¹⁶ Also, microspheres decorated with different materials (e.g., TiO₂, ZnO) can be combined in solution to form hybrid sensing films. Likewise, microspheres can be decorated with multiple layers containing different materials, which could show unique sensing properties.

In this work, we examined the sensor performance of porous 3-D nanoparticle films composed of interconnected hollow microspheres with porous antimony-doped tin oxide (Sb:SnO₂) walls. The hollow microspheres were fabricated via the layer-by-layer deposition of polyelectrolytes and nanoparticles on the surface of polystyrene latex microspheres which serve as sacrificial templates. Sensing films were then formed on the micro-hot-plate platform via drop deposition of diluted colloidal suspensions composed of Sb:SnO₂ nanoparticle-decorated microspheres and subsequent heating (to remove the latex). Sensor performance was tested in the presence of various analytes at different sensor operating temperatures. We also compared the sensitivity of such films with those of SnO₂ films prepared by CVD and with those of Sb:SnO₂ microporous films.

2. Experimental Setup

2.1. Materials System. Antimony-doped (7% mass fraction) tin oxide (Sb:SnO₂) nanoparticles (Alfa Aesar, Wand Hill, MA)¹⁷ with a density of 6.18 g/mL, a specific surface area of 104 m²/g, and an average particle diameter of ~10 nm served as the source sensing material. Sulfate-terminated latex polystyrene micro-

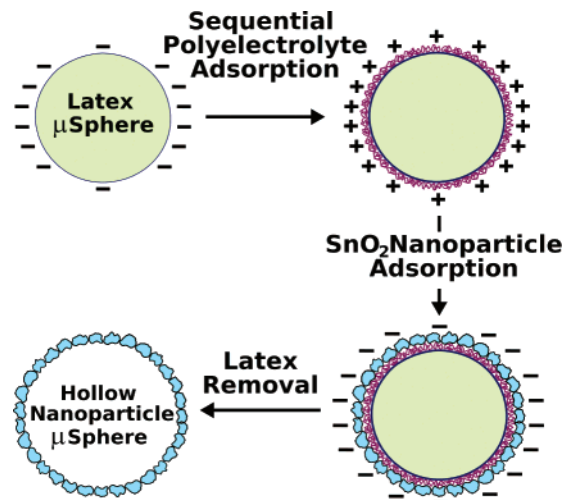


Figure 1. Schematic illustration of the layer-by-layer deposition method.

spheres (Polybead, Polysciences, Warrington, PA)¹⁷ with a density of 1.05 g/mL and an average diameter of 1.05 ± 0.01 μm served as the microsphere templates. Two polymers were used to reverse the surface charge of the latex microspheres, the positively charged poly(diallyldimethylammonium chloride) (PDADMAC; $M_w < 200000$; Aldrich, Milwaukee, WI),¹⁷ and the negatively charged poly(styrenesulfonate, sodium salt) (PSS; $M_w = 70000$; Fluka, Buchs SG, Switzerland).¹⁷

2.2. Suspension Preparation. Figure 1 shows a schematic illustration of the LbL deposition method. Our procedure is based on the work of Caruso et al.,¹⁸ and the first step involves the deposition of a three-layer polyelectrolyte film (PDADMAC/PSS/PDADMAC) onto negatively charged latex microspheres. This film provides a positively charged surface that facilitates the electrostatic adsorption of negatively charged Sb:SnO₂ nanoparticles. The PDADMAC/PSS/PDADMAC film was formed by the alternate adsorption of PDADMAC and PSS from aqueous solutions. Appropriate amounts of polyelectrolyte and latex microspheres were mixed in a 0.5 M NaCl (Sigma-Aldrich, Saint Louis, MO)¹⁷ aqueous solution to make a 10 mL suspension with 0.01% polyelectrolyte and 0.1% microsphere volume fractions. Nonadsorbed polyelectrolyte was removed by six repeated centrifugation (3000 rpm)/wash/redispersion cycles. Electrophoretic mobility measurements revealed that the polyelectrolyte trilayer had a ζ potential of approximately 36 mV. The layer thickness has been reported in the literature to be approximately 5 nm.¹⁸ The Sb:SnO₂ nanoparticle layer was deposited by adding 100 μL of a 1% volume fraction nanoparticle solution to the trilayer polyelectrolyte/latex suspension. Excess nanoparticles and NaCl were removed via six repeated centrifugation (3000 rpm)/wash/redispersion cycles with DI-H₂O, preadjusted to pH 8.5. The final suspension (0.1% volume fraction) is composed of Sb:SnO₂ nanoparticle-decorated latex microspheres (μspheres).

2.3. Micro-Hot-Plate Sensor Platform. The sensor performance of the hollow Sb:SnO₂ nanoparticle microsphere films was tested using a micro-hot-plate (μHP) sensor platform. Micro-hot-plates are MEMS devices that were designed using CMOS technology at the National Institute of Standards and Technology and then fabricated in wafer runs at the MIT Lincoln Laboratories.¹⁷ While the μHP platform has been described elsewhere,^{19,20} we briefly highlight some of its most prominent features. Figure 2a shows an SEM micrograph of a clean μHP. The μHP structure is suspended on top of a pyramidal opening (etch pit) in the Si substrate. An exploded 3-D illustration of the multilayered structure is shown in Figure 2b. A serpentine polysilicon heater is embedded within two electrically insulating

(15) Shimizu, Y.; Hyodo, T.; Egashira, M. *Catal. Surv. Asia* **2004**, *8*, 127.

(16) Suehle, J.; Cavicchi, R. E.; Gaitan, M.; Semancik, S. *IEEE Electron Device Lett.* **1993**, *14*, 118.

(17) Certain commercial instruments and suppliers are identified to adequately specify the experimental procedure. In no case does such identification imply endorsement by the National Institute of Standards and Technology.

(18) Caruso, F.; Lichtenfeld, H.; Giersig, M.; Möhwald, H. *J. Am. Chem. Soc.* **1998**, *120*, 8523.

(19) Semancik, S.; Cavicchi, R. *Acc. Chem. Res.* **1998**, *31*, 279–287.

(20) Semancik, S.; Cavicchi, R. E.; Wheeler, M. C.; Tiffany, J. E.; Poirier, G. E.; Walton, R. M.; Suehle, J. S.; Panchapakesan, B.; Devon, D. L. *Sens. Actuators, B* **2001**, *77*, 579.

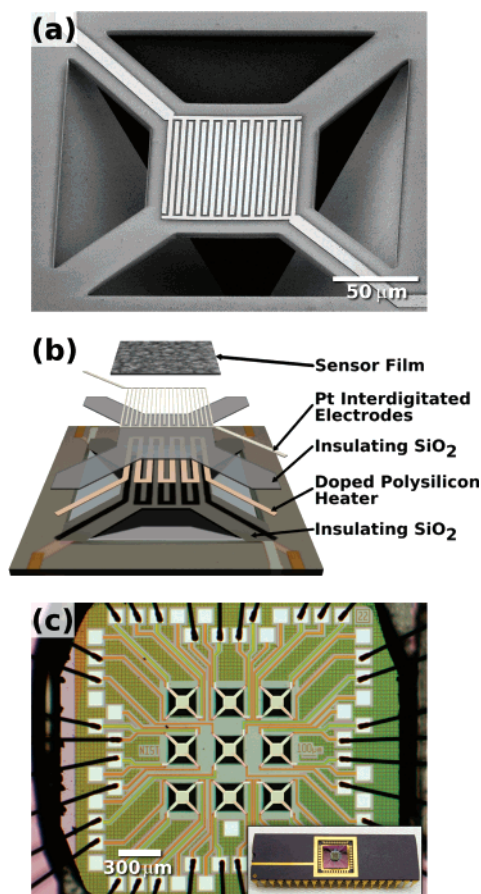


Figure 2. (a) SEM micrograph of a single μ HP. (b) Exploded 3-D schematic of the μ HP layered structure. (c) Optical image of a nine-element μ HP device. The inset shows a photograph of the nine-element micro-hot-plate device wire-bonded to a 40-pin dual in-line package.

SiO_2 layers several micrometers in thickness. The platinum interdigitated electrodes lie on top of the second SiO_2 layer. Each of the electrodes' digits are $2\ \mu\text{m}$ in width, and they have a center-to-center separation of $4\ \mu\text{m}$. The suspended sensing structure has a $100\ \mu\text{m} \times 100\ \mu\text{m}$ area and a mass of $\sim 0.2\ \mu\text{g}$. Due to their low thermal mass, these structures can be heated at rates up to 10^5 to $10^6\ \text{°C/s}$ and achieve a maximum temperature in excess of $500\ \text{°C}$. A μ HP array can be easily designed to contain anywhere from 4 to 36 of individually addressable μ HPs. The type of nine-element μ HP array used in these studies is shown in Figure 2c. To conveniently control the μ HP temperatures and monitor conductance changes from microsphere Sb:SnO_2 films deposited on the μ HP elements, the chips were packaged and wire-bonded in a standard 40-pin dual-in-line package; see Figure 2c (inset). For improved electrical contact and adhesion, the μ HPs were cleaned prior to deposition via ion beam sputtering for 3 min using a 300 V, 12 mA beam at a working distance of 10 cm.

2.4. Film Deposition and Latex Removal. Sensor films were fabricated on the μ HPs by depositing 5 nL drops of the Sb:SnO_2 nanoparticle-decorated latex microsphere solution using a micropipettor fitted with a $75\ \mu\text{m}$ internal diameter flexible tip. The micropipettor was fixed at a 45° angle to an xyz stage set to the side of an optical microscope. The tip was brought into focus using the stage, while a μ HP element was placed beneath the tip using the xy stage of the microscope. With the tip above the μ HP, a drop several hundred micrometers in diameter, was extruded from the tip, where it remained suspended. Placing a drop of such a large volume on the μ HP will produce a film that extends beyond the targeted area. Therefore, the drop is allowed to shrink, through evaporation, to a diameter close to the outer diameter of the tip. At this point, the tip is lowered until the drop comes into contact with the μ HP. The suspension then spreads to cover the μ HP, and the microspheres assemble into a continuous film. The original suspension was diluted by half

($\sim 0.05\%$ volume fraction) to compensate for the increase in solids content as the drop evaporated. While most of the water evaporated from the films in seconds after deposition, the films were allowed to fully dry in ambient conditions for 24 h before further processing. The sacrificial latex microspheres were removed by rapidly raising the temperature ($10^4\ \text{°C/s}$) of a given μ HP to $375\ \text{°C}$ using its embedded heater. This rapid heating rate and temperature were found to effectively prevent latex deformation before removal. The targeted temperature was reached in $\sim 3\ \text{ms}$ by applying 7.0–7.5 V to the embedded heaters. The heater was then maintained at $375\ \text{°C}$ for 30 min, followed by annealing at $450\ \text{°C}$ for another 30 min. The films were then cooled to room temperature and stored in ambient conditions for future testing.

2.5. CVD and Microporous Nanoparticle Films. Two other types of tin oxide films were also deposited on the μ HPs to allow performance comparisons. Films fabricated using CVD were produced by following procedures described elsewhere.²¹ Briefly, anhydrous tin(IV) nitrate was used as the tin oxide precursor. μ HPs were placed in a vacuum deposition chamber, in which a precursor flow was set using a 10 mL/min Ar carrier gas. Films were grown on individual sensor elements by heating to $375\ \text{°C}$ and monitoring the resistance of each of the films as it formed. The film growth time was 45 s, and the film resistance values in air were approximately 10 k Ω .

Compact microporous films were deposited also on μ HPs using the same nanoparticles and micropipetting technique described for the microsphere films. Aqueous (pH 8.5) suspensions containing 0.75% and 1% volume fraction nanoparticle and methyl cellulose concentrations, respectively, were employed, and methyl cellulose was added to the suspension to improve the deposition by increasing the solution viscosity and acting as a binder to prevent cracking during drying. After being dried for 24 h, the films were annealed by raising the temperature to $450\ \text{°C}$ at a rate of $100\ \text{°C/min}$ and then holding that temperature for 45 min.

BET porosimetry (Autosorb-1, Quantachrome Instruments, Boynton Beach, FL)¹⁷ measurements were performed on microporous nanoparticle films similar to those deposited on the micro-hot-plate. Films were fabricated by depositing 500 μL of the nanoparticle/methyl cellulose/water suspension on a series of 1 in. \times 1 in. glass slides. The larger substrates allowed us to collect a sufficient mass of the microporous nanoparticle material for BET measurements. These films were allowed to dry for 24 h followed by annealing for 45 min using a benchtop hot plate preheated to $450\ \text{°C}$. The BET sample was obtained by carefully removing the films from the glass slides.

2.6. Sensor Measurement Setup. Sensor response measurements were performed in a computer-controlled flow system fitted with a two-stage dilution that allows gas concentration in the range of 5 nmol/mol (5 ppb) to over 1000 $\mu\text{mol/mol}$ (1000 ppm), depending on the source gas concentration. Computer-based control was used to vary the temperature of the μ HPs and acquire electrical conductance response signals from the films deposited on them. All test measurements were performed in a dry air background. The microsphere sensors were tested against four target gases: methanol, carbon monoxide, benzene, and water. Methanol, carbon monoxide, and benzene each had a source concentration of 1000 $\mu\text{mol/mol}$, and the tested concentrations were 50, 100, 200, 400, 500, and 1000 nmol/mol. Water was generated by passing dry air through a bubbler filled with $\text{DI-H}_2\text{O}$ (at room temperature), and the tested concentrations were 5, 10, 20, 30, 40, 50, 60, 80, and 100 $\mu\text{mol/mol}$. In all cases, the background gas (dry air) was flowed through the sample chamber between analyte concentration changes. The μ HP temperature was varied during response studies from 300 to 450 °C , in increments of 50 °C .

3. Results and Discussion

3.1. Film Characteristics. For gas sensing, films should have certain morphological, structural, and electrical characteristics to maximize their performance. To increase the active surface area, the nanoparticle shell

(21) Taylor, C. J.; Semancik, S. *Chem. Mater.* **2002**, *14*, 1671–1677.

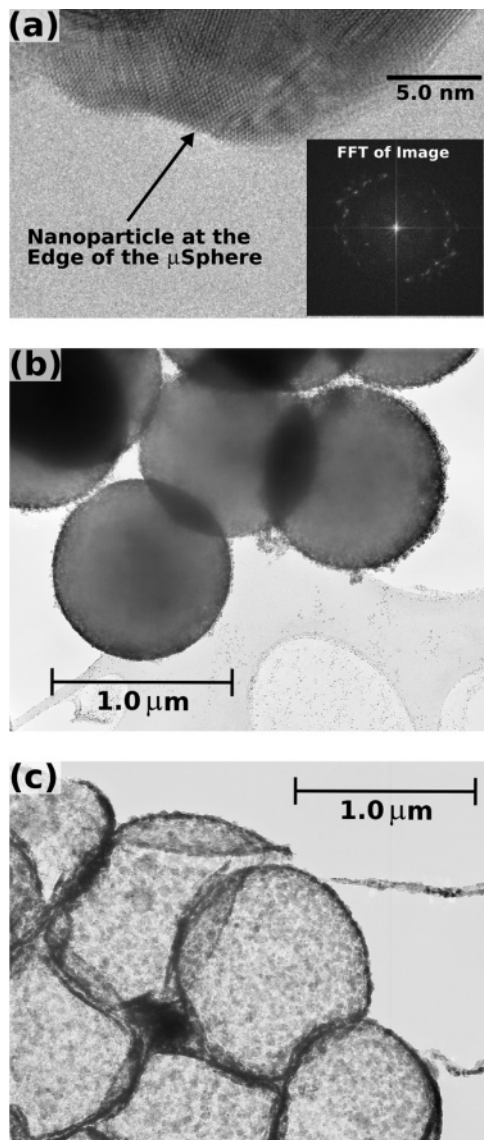


Figure 3. TEM micrographs of (a) Sb:SnO₂ nanoparticles at the edge of an Sb:SnO₂ nanoparticle-decorated microsphere before latex removal, (b) a group of Sb:SnO₂ nanoparticle-decorated latex microspheres, and (c) a group of hollow Sb:SnO₂ nanoparticle microspheres.

should be thin and porous. This ensures that both exterior and interior surfaces of the hollow microspheres are accessible to analytes. In addition, the porous shell should be sufficiently strong to support its own weight plus the weight of other nanoparticle shells. These characteristics must be achieved while maintaining good nanoparticle–nanoparticle, microsphere–microsphere, and microsphere–electrode contact to ensure proper electrical conductivity.

Figure 3 shows a series of TEM micrographs of the nanoparticle shells before and after latex removal. The micrographs were taken on a sample prepared by depositing a drop of the nanoparticle-decorated microsphere solution on a copper TEM grid. The latex microspheres were removed by placing the copper TEM grid on a bench hot plate preheated to 400 °C. Figure 3a shows a high-resolution TEM image of an Sb:SnO₂ nanoparticle that is part of the nanoparticle shell before latex removal. Both the image and the diffraction pattern (inset) in the figure highlight the crystalline nature of the nanoparticles. Similar diffraction patterns were observed after latex removal (not shown). Figure 3b shows a group of Sb:SnO₂ nanoparticle-decorated microspheres before latex removal.

The shells have a thickness of 25–50 nm, as estimated from the TEM micrographs, and they are composed of nanoparticle aggregates of similar sizes. Variations in shell thickness can be observed between the different microspheres. For example, the microsphere on the lower left of the micrograph has a thinner and smoother nanoparticle shell than the microsphere near the top right. Variation in thickness within a single microsphere can also be observed. Figure 3c shows a cluster of hollow Sb:SnO₂ nanoparticle microspheres (after latex removal). Some of the hollow microspheres have an irregular spherical shape, while other microspheres appear to have partially collapsed. Similar morphologies can be observed for films deposited on the μ HPs (see Figure 4). Partial microsphere collapse can be attributed to both the pressure exerted on the shell during the latex microsphere removal and the thickness variations in the nanoparticle shell. The collapse will likely occur in the structurally weaker, thinner regions of the nanoparticle shell. Variations in nanoparticle coverage are due to incomplete adsorption of either the polyelectrolyte and/or the nanoparticles.

Figure 4a shows an optical image of an Sb:SnO₂ nanoparticle-decorated microsphere film deposited on a μ HP. The dark gray region delineates the area covered by the film, which includes the whole sensing area and extends about halfway onto each of the μ HP support beams. No cracks are visible in the film prior to latex removal.

Figure 4b shows an optical image of the film in Figure 4a after the latex microspheres have been removed by heating. Because of the ultrathin nature of the nanoparticle shells, the films are translucent despite having an estimated overall thickness of several micrometers (\sim 4–7 μ m). Film translucency varies from almost opaque at the center to more translucent toward the perimeter of the μ HP. These translucency variations suggest that the films are thicker at the center than at the perimeter of the μ HP. Latex microspheres were not removed from the microspheres at the support beams of the μ HP. This is because the overall μ HP structure has a temperature gradient, with the temperature rapidly decreasing near the edges of the suspended platform, and then out the support beams. Figure 4c shows an SEM micrograph of the hollow Sb:SnO₂ nanoparticle microsphere film shown in Figure 4b. The film is composed of interconnected hollow Sb:SnO₂ nanoparticle microspheres with a diameter of \sim 850 nm, as determined from the SEM images. The film is contiguous within the sensing area, with cracks visible in the region where the support beams attach. Various attempts were made to measure film thickness using a profilometer without success, due to difficulties in aligning the profilometer to travel along the narrow μ HP support beams without falling into the microdevice pit and thereby damaging the profilometer tip. Figure 4d shows a higher magnification micrograph of a region of the hollow Sb:SnO₂ nanoparticle film shown in Figure 4c. The microspheres have an irregular spherical shape, and some appear to have collapsed or broken. Overall, most of the microspheres maintain their shape and there is good connectivity between them.

Besides the successful rapid heating route, we explored the use of solvents such as toluene to remove the latex microspheres. These methods were found to be ineffective because the μ HPs were prone to break during repeated washing. Different heating programs were explored as well. When the heating was initiated slowly (10² °C/min), the latex microspheres would deform before evaporating, resulting in a flattened film composed of collapsed microspheres. When the μ HP was heated rapidly (10⁴ °C/

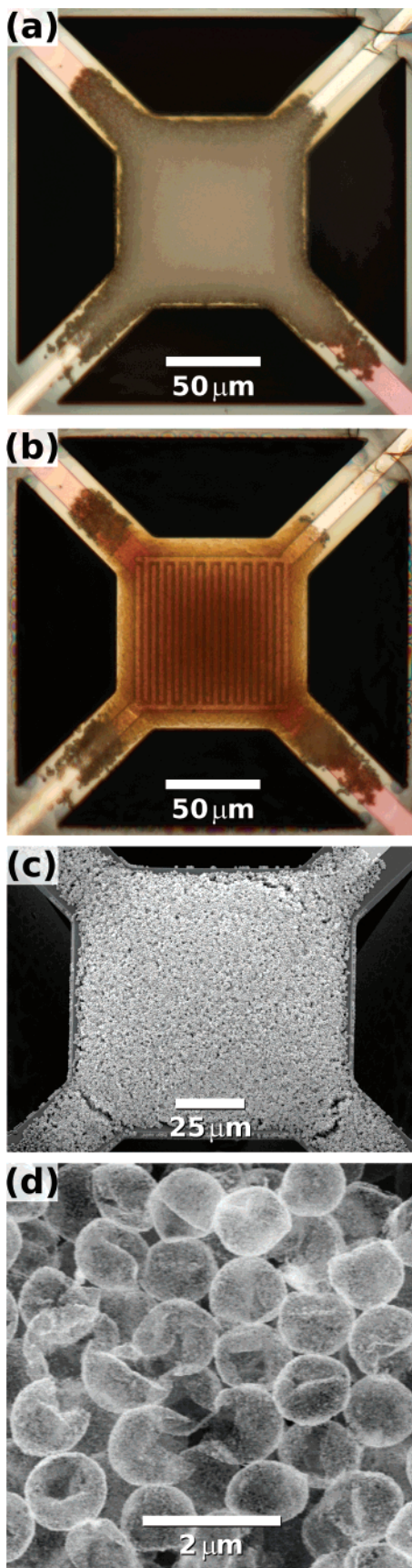


Figure 4. Optical images of (a) an Sb:SnO₂ nanoparticle-decorated latex microsphere film deposited on a μ HP and (b) a hollow Sb:SnO₂ nanoparticle microsphere film after removal of the latex microspheres via heating. SEM micrographs of (c) a hollow Sb:SnO₂ nanoparticle microsphere film on a μ HP and (d) higher magnification of the hollow Sb:SnO₂ nanoparticle microsphere film.

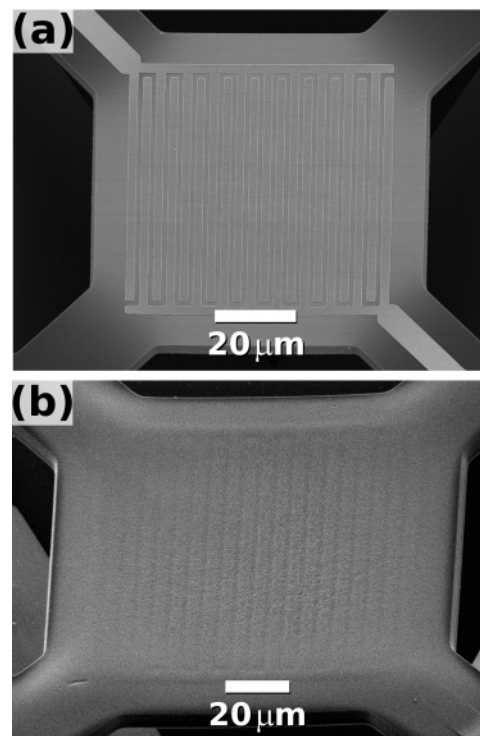


Figure 5. SEM micrographs of (a) SnO₂ CVD and (b) Sb:SnO₂ microporous nanoparticle films.

s), the microsphere shell maintained its shape. A temperature of 375 °C was chosen to ensure that the temperature through the thickness of the film was well above the 100 °C glass transition temperature of the polystyrene latex microspheres. The latex microsphere removal process occurs rapidly and is marked by an optical change from opaque to translucent, which occurs within 5 s from the moment a voltage is applied to the polysilicon heater. It is not yet clear how the latex mass is removed from the microsphere core without the nanoparticle layer being damaged. It appears that the small dimensions of the film combined with the fast heating rates lead to a “sublimation” of the latex microspheres.

Two other types of SnO₂ films were also examined in this study. Figure 5a shows an SEM micrograph of a typical polycrystalline CVD SnO₂ film deposited on a μ HP. The film is uniform within the electrode area, with a thickness of less than 100 nm and a crystallite size of \sim 10 nm. The light gray area that traverses the electrodes delineates the area of film coverage. Figure 5b shows an SEM micrograph of a microporous Sb:SnO₂ nanoparticle film deposited on a μ HP. This film is contiguous across the whole sensing area and extends onto the μ HP support beams. The thickness varies from 150 nm at the center of the μ HP to 300 nm near the perimeter, as estimated from the SEM images.

BET measurements showed that the microporous films (fabricated using the glass slide approach) have a surface area of 104 m²/g, an average pore radius of 2.35 nm, and a \sim 43% pore volume fraction. We note that BET measurements could not be performed effectively on the microsphere or CVD films whether they are deposited on micro hot plates or glass slides. The CVD films are 100% dense and have a surface area comparable to the sensing area, \sim 100 μ m \times 100 μ m. In the case of the microsphere films we calculated that they are \sim 90% porous. In this calculation we assumed that the films are composed of close-packed hollow microspheres with an internal di-

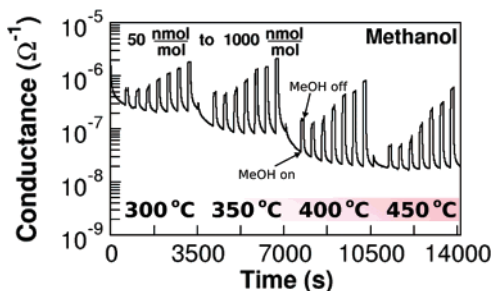


Figure 6. Conductance response of the hollow Sb:SnO₂ nanoparticle microspheres film to methanol at different temperatures. The concentrations used for methanol were 50, 100, 200, 400, 500, and 1000 nmol/mol.

ameter of 800 nm and a nanoparticle shell that is 43% porous and has a thickness of 50 nm.

3.2. Sensing Performance. Sensors are typically evaluated on four key performance aspects: sensitivity, selectivity, stability, and speed. In this work we looked at the first three starting with sensitivity. Sensitivity is defined as the ratio of film conductance in the presence of a gas to the baseline conductance measured in dry air ($S = G/G_0$). In addition, we examined aspects of selectivity, which is defined as the ability of the sensor to differentiate between analytes. Finally, we looked at the film stability by monitoring the baseline and signal response levels over time during exposure to on–off cycles consisting of various concentrations of analytes (“on”) and dry air (“off”). All the performance parameters were tested by measuring changes in conductance at different analyte concentrations at elevated temperatures.

Figure 6 shows the typical response of a hollow Sb:SnO₂ nanoparticle microspheres film to different methanol concentrations at different temperatures. The measurements were done by holding the film at a fixed temperature while measuring the sensing response to different methanol concentrations of 50, 100, 200, 400, 500, and 1000 nmol/mol. The process was repeated for four temperatures ranging from 300 to 450 °C, in 50 °C increments. These temperatures fall within the typical range used with Sb:SnO₂ films for sensor applications.³ The plot shows a series of upward spikes in conductance that indicate the period of time when the analyte is introduced into the sample chamber. There was an increase in conductivity upon the introduction of the analyte (on), followed by a decrease to baseline once the analyte was turned off. The baseline conductance decreased with temperature, while the sensitivity to a given analyte concentration increased with temperature. For example, the baseline conductance decreased from $10^{-7} \Omega^{-1}$ at 300 °C to $10^{-8} \Omega^{-1}$ at 400 °C, while the sensitivity (G/G_0) for a 1000 nmol/mol concentration increased from 8 to 40 at these temperatures. The increase in sensitivity with temperature can arise due to the nature of the energetics and kinetics of surface interactions. However, the decrease in baseline conductance with increasing temperature does not follow the expected trend of increasing conductance with temperature. A measurement of conductance as a function of time and temperature between 100 and 450 °C (not shown) indicated that the baseline conductance for these films increased to a maximum at a temperature of 300 °C. Beyond this temperature, the baseline conductance decreased in a fashion similar to that shown in Figure 6. Similar behavior (but with a different transition point) has been observed for antimony-doped nanoparticle films as reported by Bommel et al.²² Below 700 °C they observed a conductance increase with temperature, but at higher temperatures the conductance decreased. They attributed

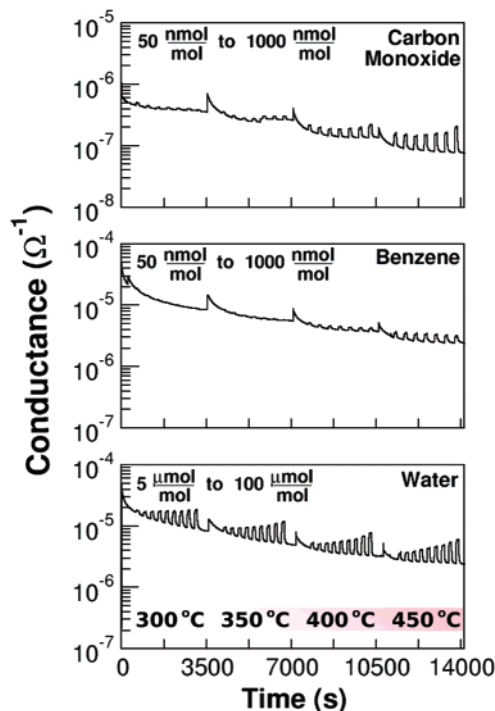


Figure 7. Conductance responses of the hollow Sb:SnO₂ nanoparticle microspheres film to different gases at different temperatures. The concentrations used for carbon monoxide and benzene were 50, 100, 200, 400, 500, and 1000 nmol/mol. The water concentrations were 5, 10, 20, 30, 40, 50, 60, 80, and 100 μ mol/mol.

this behavior to an irreversible migration of antimony to the surface of the nanoparticles. In our case, this does not seem like a possible explanation because the transition that we observed is reversible and occurs at a much lower temperature. We note that the decrease in conductance above 300 °C was also observed for the Sb:SnO₂ microporous nanoparticle and SnO₂ CVD films (see Figure 9) that were examined in these studies. Further research is needed to understand this behavior.

We performed basic measurements of selectivity, by testing the sensor response to different analytes (at different concentrations and temperatures). Figure 7 shows the response of the hollow Sb:SnO₂ nanoparticle film to carbon monoxide, benzene, and water. The carbon monoxide and benzene concentrations tested were 50, 100, 200, 400, 500, and 1000 nmol/mol. The water was measured at concentrations of 5, 10, 20, 30, 40, 50, 60, 80, and 100 μ mol/mol. The different concentration range for water was necessitated by the inability of the water generator used in this study to reliably deliver a nanomole per mole concentration of water vapor. The same film was examined for all of the analytes and concentrations. The magnitude of the response (sensitivity) for a given concentration varied among the different analytes. In addition, there were variations in the μ HP temperature that produced maximum sensitivity for the different analytes. For example, for H₂O the film shows well-defined, large changes in conductance at the lowest temperature tested (300 °C), while the response to benzene and CO was suppressed until a 400 °C operating temperature was reached. This behavior is expected since the film reactivity to different analytes varies with temperature.¹⁹ These sensitivity differences with varying temperatures can offer some degree of specificity to various analytes. It is possible

(22) Bommel, M. J. V.; Groen, W. A.; van Hal, H. A. M.; Keur, W. C.; Bernards, T. N. M. *J. Mater. Sci.* **1999**, *34*, 4803.

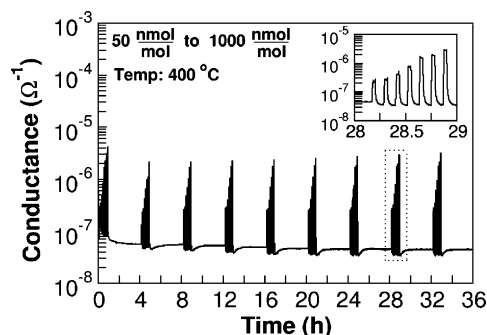


Figure 8. Long-term test of the stability of a hollow SnO_2 nanoparticle microsphere film exposed to methanol. The inset shows an enlarged view of the run at the 28th hour. The temperature was held at $400\text{ }^\circ\text{C}$ during the test.

to combine temperature-driven specificity with multiple-material orthogonality to produce a type of “fingerprint” of a given analyte.^{3,19} This could be achieved by depositing different materials on the different μHPs in a device. Each film will respond differently to an analyte at different temperatures. This information can be used by neural network algorithms to identify individual analytes within a mixture.²³ In general, the hollow $\text{Sb}:\text{SnO}_2$ nanoparticle microsphere films show good partial selectivity for the different gases.

The stability of the hollow $\text{Sb}:\text{SnO}_2$ nanoparticle microsphere films was tested by monitoring the sensor response to methanol at regular intervals and at a constant temperature over several hours. Figure 8 shows the long-term response to methanol of the hollow $\text{Sb}:\text{SnO}_2$ nanoparticle microsphere film. The tests were performed by measuring changes in conductivity at different methanol concentrations (50, 100, 200, 400, 500, and 1000 nmol/mol) every 4 h while keeping the temperature at $400\text{ }^\circ\text{C}$ for a total of 36 h. The inset in Figure 8 shows an expanded view of the test done between the 28th and 29th hours. It shows that the film conductance increased upon the analyte introduction and decayed to a constant baseline once the analyte was turned off. The film baseline conductance decayed almost 1 order of magnitude, from 3×10^{-7} to $4.5 \times 10^{-8}\ \Omega^{-1}$, during the first 20 h of the test. Most of the change in baseline conductance (90%) occurred during the first 3 h. This period of baseline conductance stabilization was observed for all $\text{Sb}:\text{SnO}_2$ and SnO_2 films. It was also seen in every sensor test performed after the μHP device was stored at room temperature. The film exhibited good repeatability and dynamic range during the length of the test. The sensitivity (magnitude of response) to a given concentration was repeatable throughout the test. Films similar to those used here showed good stability after 30 days of intermittent testing.

The sensitivity of the hollow $\text{Sb}:\text{SnO}_2$ nanoparticle microsphere film to different analytes was compared to those of a SnO_2 CVD film and a $\text{Sb}:\text{SnO}_2$ microporous nanoparticle film. The three films were deposited within the same nine-element μHP array and were tested simultaneously. The CVD film is not antimony-doped; therefore, it is not possible to make a direct comparison in terms of morphological effects alone. Despite this, they represent some of the highest quality device films made in our laboratory, and therefore, they offer a good gauge to measure the overall sensitivity performance of the microsphere films. The microporous and hollow microsphere film microstructures can be compared directly since

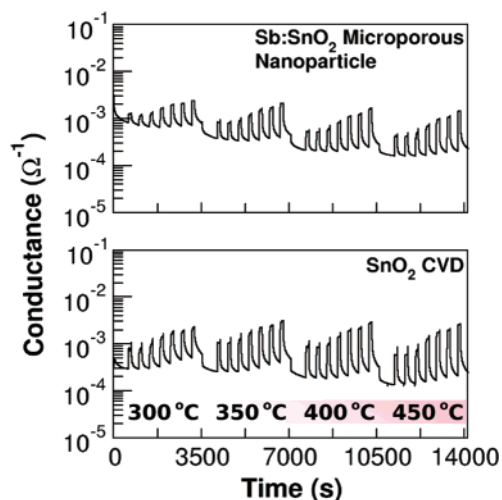


Figure 9. Conductance response of the $\text{Sb}:\text{SnO}_2$ microporous nanoparticle and SnO_2 CVD films to methanol at $400\text{ }^\circ\text{C}$. The concentrations used for methanol were 50, 100, 200, 400, 500, and 1000 nmol/mol.

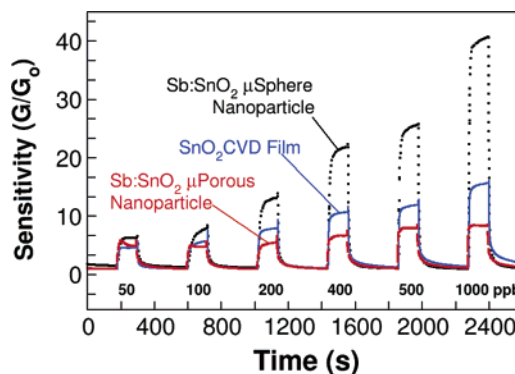


Figure 10. Sensitivity (to methanol) comparison of a hollow $\text{Sb}:\text{SnO}_2$ nanoparticle microsphere film, a SnO_2 CVD film, and an $\text{Sb}:\text{SnO}_2$ microporous nanoparticle film. Sensitivity was obtained by dividing the conductance (G) by the baseline conductance (G_0). All films were tested within a single nine-element μHP array device.

they were fabricated with the same $\text{Sb}:\text{SnO}_2$ nanoparticles. Figure 9 shows the conductance response of the $\text{Sb}:\text{SnO}_2$ microporous nanoparticle and SnO_2 CVD films to different methanol concentrations (50–1000 nmol/mol) and different temperatures (300– $450\text{ }^\circ\text{C}$). Both the microporous and CVD films exhibit similar response dependence on temperature and methanol concentration when compared to the microsphere film. There is an increase in conductivity upon the introduction of the analyte (on), followed by a decrease to baseline once the analyte is turned off. Also the sensitivity increases with temperature and analyte concentration, and the baseline conductance decreases with increasing temperature. Overall, the three films tested show similar response dependence on temperature and concentration to methanol, carbon monoxide, benzene, and water. Their analogous behavior indicates that the conductivity changes arise from the same type of surface mechanism, which involves the interaction of the analyte species at elevated temperatures with the oxidized tin oxide surface. The main difference between these films is that the microporous film shows higher sensitivities to the different analytes tested, in particular when compared with the microsphere film. The enhancement in sensitivity can be better appreciated in Figure 10, which shows a plot comparing the sensor sensitivity to methanol at $400\text{ }^\circ\text{C}$ for the $\text{Sb}:\text{SnO}_2$ microsphere

(23) Boger, Z.; Mier, D. C.; Cavicchi, R. E.; Semancik, S. *Sens. Lett.* **2003**, *1*, 86.

Table 1. Sensitivities for a Hollow Sb:SnO₂ Nanoparticle Microsphere Film, an Sb:SnO₂ Microporous Nanoparticle Film, and a SnO₂ CVD Film to Methanol, Carbon Monoxide, and Benzene at a Concentration of 1000 nmol/mol and Water at a Concentration of 100 μmol/mol^a

gas	μsphere	μporous	CVD
methanol	40.3	8.2	15.5
carbon monoxide	1.6	1.0	1.1
benzene	1.2	1.0	1.2
water	2.3	1.3	1.5

^a All sensitivities are reported at a temperature of 400 °C.

nanoparticle, Sb:SnO₂ microporous nanoparticle, and SnO₂ CVD films. Six concentrations were tested from 50 to 1000 nmol/mol. The hollow Sb:SnO₂ nanoparticle microsphere film showed higher sensitivity to methanol than both the CVD and microporous films across the whole range of concentrations tested. For example, at a concentration of 1000 nmol/mol, the hollow microsphere film was 2.6 and 4.9 times more sensitive than the CVD and microporous films, respectively. Table 1 summarizes the sensitivities of the three films to methanol, carbon monoxide, and benzene at a concentration of 1000 nmol/mol and water at a concentration of 100 μmol/mol (all at 400 °C). Sensitivities to carbon monoxide, benzene, and water are relatively small compared to that to methanol, for all films tested. This is expected since these analytes do not interact as strongly with the tin oxide surface; therefore, enhancements due to increases in surface area are suppressed. Despite this, the microsphere film showed sensitivities equal to or higher than those of the microporous and CVD films to all the analytes tested.

The high sensitivities observed for the hollow microsphere films highlight the benefits of an open porous architecture. Porosity and pore radius can have a large effect on analyte diffusion. If we assume that the diffusion through a particle bed follows a Knudsen flow, then in its most elemental form the diffusion coefficient is proportional to the pore radius as defined by the following equation:²⁴

$$D_K = \frac{2}{3} \frac{\epsilon}{\tau} r \left(\frac{8RT}{\pi M} \right)^{1/2}$$

where D_K is the Knudsen diffusion coefficient in a porous medium, ϵ is the dimensionless porosity, τ is the dimensionless tortuosity, r is the pore radius, R is the universal gas constant, T is the temperature, and M is the molar mass. The gas diffusion is directly proportional to the porosity and pore radius and inversely proportional to the pore network tortuosity. BET porosimetry reveals that the microporous nanoparticle films (see Figure 5) are composed of tightly packed nanoparticles with an average pore radius of 2.35 nm and 43% total porosity. These small pores combined with a tortuous compact pore network limit analyte penetration into the internal surface of the film. This restricted morphology is in sharp contrast with the hollow microsphere films, which show a multiscale porous structure. The hollow microsphere films are estimated to be ~90% porous or twice as porous as the microporous films. In addition, the pore radius is from 1 to 2 orders of magnitude higher than that of the microporous films when we consider that the interstices

between microspheres are >50 nm in radius and that the internal radius for the hollow microspheres is >700 nm. While the pore radius decreases at the surface of the hollow microspheres, it is worth noting that the nanoparticle shell contains a large degree of mesoporosity that should facilitate analyte diffusion into the microsphere interior. Because both the exterior and the interior of the microspheres are accessible to the analytes, the available active surface area is enhanced. The large increase in active surface area and analyte diffusion does not necessarily translate into a proportional increase in sensitivity however. There are other factors involved in the transduction of analyte/surface reactions into an electrical conductance change. These include the electrode/microsphere and microsphere/microsphere contacts, microsphere organization in the film, and electrical and surface properties of the electrodes. The sensitivity reported here represents the typical performance of the hollow nanoparticle microsphere films. Several hollow microsphere films (not shown) have exhibited even higher sensitivities (i.e., over 1 order of magnitude increase in sensitivity compared to that of the CVD and microporous films). The exact morphological and electrical aspects responsible for such variations in resistivity are not clear. To better understand the nature of the enhancements produced by the hollow microsphere films, future studies will examine structural parameters such as the diameter of the microspheres and film thickness. Additional types of analytes, larger concentration ranges, and response times will also be examined.

4. Conclusions

Using the layer-by-layer deposition technique, we were able to fabricate chemical sensor films composed of interconnected hollow Sb:SnO₂ nanoparticle microspheres. For the first time, this type of film was deposited on μHP sensor platforms. The rapid heating rates made possible by this platform were found to be necessary for removal of the latex microsphere templates in a manner that preserved the nanoparticle microsphere shape. Hollow microsphere films show partial selectivity for different gases, good dynamic range over different temperatures and concentrations, and good stability over long analyte exposures. These films also offer an enhancement in sensitivity to methanol, carbon monoxide, benzene, and water over microporous nanoparticle and compact CVD films. The gain in sensitivity was attributed to their multiscale porous architecture that promotes analyte diffusion and increases the available active surface area. Finally, the layer-by-layer deposition technique offers the possibility to fabricate composite nanostructured sensing films that may show novel sensing properties.

Acknowledgment. We gratefully acknowledge the help of Dr. Vincent Hackley of the Materials Science and Engineering Laboratory at NIST in performing ζ potential measurements. We thank Dr. Chiara (Clarissa) Ferraris and Mr. Max Peltz, both part of the Materials and Construction Research Division at NIST, for performing BET measurements, and Dr. Guofeng Li and Dr. Richard Cavicchi for their assistance and useful discussions. C.J.M. acknowledges financial support from the National Research Council Postdoctoral Associateship Program at NIST.

(24) Veldsink, J. W.; van Damme, R. M. J.; Versteeg, G. F.; van Swaaij, W. P. M. *Chem. Eng. J.* **1995**, *57*, 115.